

STAR-RIS-NOMA Networks: An Error Performance Perspective

Mahmoud Aldababsa, Aymen Khaleel, and Ertugrul Basar, *Senior Member, IEEE*

Abstract—This letter investigates the bit error rate (BER) performance of simultaneous transmitting and reflecting reconfigurable intelligent surfaces (STAR-RISs) in non-orthogonal multiple access (NOMA) networks. In the investigated network, a STAR-RIS serves two non-orthogonal users located on either sides of the surface by utilizing the mode switching protocol. We derive the closed-form and upper bound BER expressions in perfect and imperfect successive interference cancellation cases. Furthermore, asymptotic analyses are also conducted to provide further insights into the BER behavior in the high signal-to-noise ratio region. Finally, the accuracy of our theoretical analysis is validated through Monte Carlo simulations. The obtained results reveal that the BER performance of STAR-RIS-NOMA outperforms that of the classical NOMA system, and STAR-RIS might be a promising NOMA 2.0 solution.

Index Terms—Bit error rate, non-orthogonal multiple access, simultaneous transmitting and reflecting reconfigurable intelligent surface, successive interference cancellation.

I. INTRODUCTION

NON-ORTHOGONAL multiple access (NOMA) has been recognized as a promising multiple access candidate to satisfy the challenging requirements of sixth-generation (6G) wireless networks such as high spectral efficiency, massive connectivity, and low latency [1]. Different from conventional orthogonal multiple access (OMA), in which different users are allocated to different resource blocks (time, frequency, code), NOMA can accommodate multiple users via the same resource block, which effectively enhances the spectral efficiency. In power-domain (PD)-NOMA, users are assigned to different power levels, and the signals of all users are superimposed into a single message transmitted from the base station (BS). At the receiver side, successive interference cancellation (SIC) is applied to eliminate the inter-user interference and to recover the transmitted symbol [2].

Simultaneous transmitting and reflecting reconfigurable intelligent surfaces (STAR-RISs) are recently proposed to achieve 360° wireless coverage [3]. Compared to classical RISs, STAR-RISs can serve users located on both sides of their surface. Particularly, STAR-RISs consist of elements that can produce both electric polarization and magnetization currents, which allows simultaneous control of the transmit and reflect incident signals towards the users located at different sides of the surface.

Recently, a number of works have been reported incorporating NOMA and STAR-RIS in wireless networks to enhance the spectral efficiency and extend the coverage area [4]–[17]. Compared with conventional RISs, the authors in [4] showed

that the coverage can be significantly extended by integrating STAR-RISs into NOMA networks. The authors in [5] took advantage of STAR-RIS to simultaneously eliminate inter-cell interference and enhance the desired signals in NOMA enhanced coordinated multi-point transmission networks. In [6], the authors considered an optimization problem to maximize the achievable sum-rate of STAR-RIS-NOMA systems by jointly optimizing power allocations, decoding order, and both active and passive beamforming vectors. The STAR-RIS in [7] is utilized for adjusting users' decoding order to efficiently mitigate the mutual interference between users and to extend the coverage of heterogeneous networks, which incorporates NOMA with the over-the-air federated learning. In [8] and [9], the authors proposed different approximated mathematical channel models to investigate the outage probability (OP) performance for STAR-intelligent omni-surfaces (STAR-IOSs) based NOMA and STAR-RIS-NOMA multi-cell networks. In [10], the authors considered a realistic transmission and reflection coupled phase-shift model for STAR-RISs. Based on this model, a power consumption minimization problem is formulated and solved using alternating optimization. The authors in [11] proposed a STAR-RIS partitioning algorithm for a downlink STAR-RIS-NOMA network. More specifically, the proposed algorithm is designed to maximize the sum-rate and guarantee the quality-of-service requirements by assigning a proper number of STAR-RIS elements to each user. In [12] and [13], optimizations problems are considered to minimize the power consumption and maximum secrecy OP, respectively, for uplink STAR-RIS-NOMA networks. The authors in [14] investigated the resource allocation scheme in STAR-RIS-aided multi-carrier OMA and NOMA networks to maximize the system sum-rate. In [15], a deep reinforcement learning-based algorithm is designed to maximize the energy efficiency for a STAR-RIS-NOMA network. The authors in [16] proposed practical phase-shift configuration (PSC) strategies for STAR-RIS-NOMA networks with correlated phase shifts. Then, the OP and power scaling law are derived for each proposed PSC strategy. In [17], the performance of STAR-RIS-NOMA networks is investigated in terms of OP and ergodic sum-rate in the cases of perfect and imperfect SIC.

To the best of the authors' knowledge, so far, the performance of STAR-RIS-NOMA networks are only analyzed in terms of OP and sum-rate, and no light has been shed on the bit error rate (BER) performance aspect yet. This has motivated us to investigate the BER performance for STAR-RIS-NOMA networks, where BS communicates two non-orthogonal users with the assistance of a STAR-RIS. The main contributions of the paper can be summarized as follows. We analyze the BER

performance of the STAR-RIS-NOMA network in the cases of perfect and imperfect SIC. Specifically, we derive the closed-form expressions of the BER and its corresponding upper bound for both users. Then, asymptotic analyses are carried out to provide further insight into BER behavior in the high signal-to-noise ratio (SNR) region. Finally, we verify our analytical results by Monte Carlo simulations, which demonstrate the superiority of the proposed STAR-RIS-NOMA network over the classical NOMA system.¹

II. SYSTEM MODEL

As illustrated in Fig. 1, we consider a STAR-RIS-NOMA network, in which a single-antenna BS communicates simultaneously two single-antenna users with the help of an STAR-RIS equipped with N passive elements. The two users are deployed on both sides of the STAR-RIS, where the users located in the transmission and reflection zones are denoted, respectively, by U_t and U_r . The direct communication links between the BS and users are assumed to be blocked by obstacles and the STAR-RIS is deployed to provide alternative communication links for users through the transmission/reflection elements. The STAR-RIS adopts mode switching (MS) protocol, where each element can operate in full transmission or reflection mode. Thus, the STAR-RIS is partitioned into two main parts, where the first and second parts contain N_t and N_r elements to serve the users in transmission and reflection zones, respectively. The elements in the first and second parts are operated in the transmission and reflection modes, respectively, and the STAR-RIS is assumed to be deployed in the far-field of the BS. The BS-STAR-RIS link is assumed to follow Rayleigh fading channel model, where $\mathbf{h}_k \in \mathbb{C}^{N_k \times 1}$ denotes the BS-STAR-RIS channel vector with $k \in \{t, r\}$ denotes the transmission (t)/reflection (r) user. $\mathbf{h}_k = [h_k^{(1)}, \dots, h_k^{(n)}, \dots, h_k^{(N_k)}]^T$ with $h_k^{(n)} = \sqrt{L_{BS}} \zeta_k^{(n)} e^{-j\phi_k^{(n)}}$ denoting the channel coefficient between the BS and n th STAR-RIS element in the t/r part, where L_{BS} , $\zeta_k^{(n)}$, and $\phi_k^{(n)}$ denote the path gain, channel amplitude, and channel phase, respectively, and $h_k^{(n)} \sim \mathcal{CN}(0, L_{BS})$. Likewise, the STAR-RIS- U_k link is assumed to follow Rayleigh fading channel model, where the channel vector between the transmission or reflection part of the STAR-RIS and U_k is denoted by $\mathbf{g}_k \in \mathbb{C}^{N_k \times 1}$, $\mathbf{g}_k = [g_k^{(1)}, \dots, g_k^{(n)}, \dots, g_k^{(N_k)}]^T$, $g_k^{(n)} = \sqrt{L_{SU,k}} \eta_k^{(n)} e^{-j\Phi_k^{(n)}}$ denotes the channel coefficient between n th RIS element and U_k , where $L_{SU,k}$, $\eta_k^{(n)}$, and $\Phi_k^{(n)}$ denote the path gain, channel amplitude, and channel phase, respectively, and $g_k^{(n)} \sim \mathcal{CN}(0, L_{SU,k})$. The transmission and reflection coefficients for the transmission and reflection parts of the STAR-RIS are denoted by the entries of the diagonal matrix $\Theta_k \in \mathbb{C}^{N_k \times N_k}$, for the n th element we have

¹Notation: Matrices and vectors are denoted by an upper and lower case boldface letters, respectively. $\mathbb{C}^{m \times n}$ denotes the set of matrices with dimension $m \times n$. $|\cdot|$, $\mathbb{E}[\cdot]$, and $(\cdot)^T$ represent the absolute value, expectation operator, and transpose operator, respectively. $f_X(x)$ denotes probability density function (PDF) of a random variable (RV) X . $\mathcal{CN}(\mu, \sigma^2)$ stands for the complex Gaussian distribution with mean μ and variance σ^2 . $Q(\cdot)$ and $\text{erf}(\cdot)$ denote the Q -function and error function, respectively.

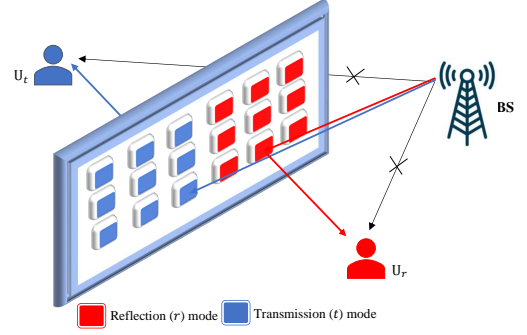


Fig. 1. A STAR-RIS assisted NOMA system model.

$\Theta_k^{(n,n)} = \beta_k^{(n)} e^{j\theta_k^{(n)}}$, where $\theta_k^{(n)} \in [0, 2\pi)$ and $\beta_k^{(n)} = 1$, under the full transmission/reflection assumption.

In the considered setup, U_t and U_r are considered to have the weakest and strongest channel gains, respectively. Thus, according to PD-NOMA protocol, the power allocation for U_t and U_r are a_t and a_r , respectively, where $a_t \geq a_r$. Given, P is the BS transmit power, x_k and a_k are U_k 's symbol and power allocation factor, respectively, $\mathbb{E}[|x_k|^2] = 1$, $\sum_k a_k = 1$. Then, the BS transmits the superimposed signal $x = \sum_k \sqrt{a_k P} x_k$ to all users and the received signal at U_k is

$$y_k = \mathbf{g}_k^T \Theta_k \mathbf{h}_k x + n_k, \quad (1)$$

where n_k denotes the complex additive white Gaussian noise (AWGN) sample with zero mean and variance σ^2 at U_k , i.e., $n_k \sim \mathcal{CN}(0, \sigma^2)$.

III. BIT ERROR RATE ANALYSIS

In this section, we derive theoretical expressions of the BER for each user in the perfect and imperfect SIC scenarios. Then, we obtain the corresponding upper bound BER expressions and BER behavior in the high SNR region.

In general, the average bit error probability for U_k in fading channels is given by

$$\mathcal{P}_{e,k} = \int_0^\infty \mathcal{P}(e|\varphi_k) f_{\varphi_k}(x) dx, \quad (2)$$

where $\varphi_k = |\mathbf{g}_k^T \Theta_k \mathbf{h}_k|$, $\mathcal{P}(e|\varphi_k)$ and $f_{\varphi_k}(x)$ denote absolute cascaded channel, conditional BER for U_k in AWGN channel and the PDF of the cascaded channel φ_k , respectively. In what follows, we derive $\mathcal{P}(e|\varphi_k)$ and $f_{\varphi_k}(x)$ in Lemma 1 and Lemma 2, respectively, then we obtain $\mathcal{P}_{e,k}$ in Proposition 1.

Lemma 1. The BER for U_k in AWGN can be given by

$$\mathcal{P}(e|\varphi_k) = \sum_{\mathbb{A}_k} \mathcal{P}(\mathbb{A}_k) Q\left(\mathbb{A}_k \varphi_k \sqrt{\varrho_k^{sic} \gamma}\right), \quad (3)$$

where $k \in \{t, r\}$, $\mathbb{A}_t \in \{\sqrt{a_t} + \sqrt{a_r}, \sqrt{a_t} - \sqrt{a_r}\}$, $\mathbb{A}_r \in \{\sqrt{a_r}\}$ and $\mathcal{P}(\mathbb{A}_k)$ denotes probability of \mathbb{A}_k , i.e., $\mathcal{P}(\mathbb{A}_t) = \frac{1}{2}$ and $\mathcal{P}(\mathbb{A}_r) = 1$. Additionally, $\gamma \triangleq \frac{P}{\sigma^2}$, $\varrho_k^{sic} = 1$, $\varrho_r^{sic} = \frac{1}{1 + \epsilon \Omega_r a_t \gamma}$, $\Omega_r = \mathbb{E}[\varphi_r^2]$, and $\epsilon \in [0, 1]$ denotes error propagation factor.

Proof. See Appendix A. ■

Lemma 2. The PDF of φ_k is given by

$$f_{\varphi_k}(x) = \frac{1}{\sqrt{2\pi v_k}} \exp\left(-\frac{(x - \mu_k)^2}{2v_k}\right), \quad (4)$$

where $\mu_k = \frac{\pi}{4}\sqrt{L_k}N_k$ and $v_k = \left(1 - \frac{\pi^2}{16}\right)L_kN_k$. Here, $L_k = L_{BS}L_{SU,k} = \frac{1}{d_{BS}^{\alpha_{BS}}d_{SU,k}^{\alpha_{SU}}}$ is the overall path gain of the BS-STAR-RIS- U_k link, where α_{BS} , and α_{SU} refer to path loss exponents associated with the BS-RIS and RIS- U_k links, respectively. Additionally, d_{BS} , and $d_{SU,k}$ denote the distances from BS to STAR-RIS, and STAR-RIS to U_k , respectively.

Proof. See Appendix B. ■

Proposition 1. In the perfect and imperfect SIC cases, the BER of U_k is given by

$$\begin{aligned} \mathcal{P}_{e,k} &\approx \frac{\exp\left(-\frac{2cv_k + \mu_k^2}{2v_k}\right)}{\sqrt{2v_k}} \sum_{\mathbb{A}_k} \mathcal{P}(\mathbb{A}_k) \\ &\times \exp\left(\frac{(b\mathbb{A}_k\sqrt{\varrho_k^{sic}\gamma v_k} - \mu_k)^2}{4a\mathbb{A}_k^2\varrho_k^{sic}\gamma v_k^2 + 2v_k}\right) \sqrt{\frac{v_k}{4\mathbb{A}_k^2\varrho_k^{sic}\gamma v_k + 2}} \\ &\times \left(1 + \operatorname{erf}\left(\sqrt{\frac{(b\mathbb{A}_k\sqrt{\varrho_k^{sic}\gamma v_k} - \mu_k)^2}{4a\mathbb{A}_k^2\varrho_k^{sic}\gamma v_k^2 + 2v_k}}\right)\right), \end{aligned} \quad (5)$$

where $(a, b, c) = (0.3842, 0.7640, 0.6964)$ are the fitting coefficients used by Lopez-Benitez and Casadevall in approximating Q-function [18].

Proof. See Appendix C. ■

In Proposition 1, by substituting $\varrho_r^{sic} = 1$, i.e., $\epsilon = 0$, the BER of U_k is obtained in the case of perfect SIC. It is worth mentioning that U_t has the highest allocated power coefficient and thus it does not perform SIC process while U_r needs SIC process to detect and subtract U_t 's signal. Accordingly, Proposition 1 gives the BER for U_t in the perfect SIC case and U_r in both perfect and imperfect SIC cases.

Corollary 1. In the perfect and imperfect SIC cases, the upper bound BER of U_k is given by

$$\begin{aligned} \mathcal{P}_{e,k}^b &= \frac{\exp\left(-\frac{\mu_k^2}{2v_k}\right)}{\sqrt{2v_k}} \sum_{\mathbb{A}_k} \mathcal{P}(\mathbb{A}_k) \exp\left(\frac{\mu_k^2}{2\mathbb{A}_k^2\varrho_k^{sic}\gamma v_k^2 + 2v_k}\right) \\ &\times \sqrt{\frac{v_k}{2\mathbb{A}_k^2\varrho_k^{sic}\gamma v_k + 2}} \left(1 + \operatorname{erf}\left(\sqrt{\frac{\mu_k^2}{2\mathbb{A}_k^2\varrho_k^{sic}\gamma v_k^2 + 2v_k}}\right)\right). \end{aligned} \quad (6)$$

Proof. By applying the Chernoff bound on the Q-function in Lemma 1, $\mathcal{P}(e|\varphi_k) \leq \sum_{\mathbb{A}_k} \mathcal{P}(\mathbb{A}_k) \exp\left(-\frac{\mathbb{A}_k^2\varrho_k^2\varrho_k^{sic}\gamma}{2}\right)$, then, $\mathcal{P}_{e,k}^b = \frac{\exp\left(-\frac{\mu_k^2}{2v_k}\right)}{\sqrt{2\pi v_k}} \sum_{\mathbb{A}_k} \mathcal{P}(\mathbb{A}_k) \int_0^\infty \exp\left(-\frac{\mathbb{A}_k^2\varrho_k^{sic}\gamma v_k + 1}{2v_k}x^2 + \frac{\mu_k}{v_k}x\right) dx$. Here, the integral can be written in terms of error function [19, Eq. (3.322.2)]. Therefore, the upper bound BER of U_k can be finally stated in (6), and then the proof is complete. ■

It is difficult to get an insight from the BER expression in Proposition 1. Therefore, in the following corollary, we examine the BER behavior in the high SNR regime.

Corollary 2. In the presence of imperfect SIC, when $\gamma \rightarrow \infty$, the BER can be given as

$$\begin{aligned} \mathcal{P}_{e,k}^\infty &\approx \frac{\exp\left(-\frac{2cv_k + \mu_k^2}{2v_k}\right)}{\sqrt{2v_k}} \sum_{\mathbb{A}_k} \mathcal{P}(\mathbb{A}_k) \\ &\times \exp\left(\frac{(b\mathbb{A}_k\sqrt{\varpi}v_k - \mu_k)^2}{4a\mathbb{A}_k^2\varpi v_k^2 + 2v_k}\right) \sqrt{\frac{v_k}{4\mathbb{A}_k^2\varpi v_k + 2}} \\ &\times \left(1 + \operatorname{erf}\left(\sqrt{\frac{(b\mathbb{A}_k\sqrt{\varpi}v_k - \mu_k)^2}{4a\mathbb{A}_k^2\varpi v_k^2 + 2v_k}}\right)\right), \end{aligned} \quad (7)$$

where $\varpi = (\epsilon\Omega_r a_t)^{-1}$.

Proof. Let $\varpi = \varrho_k^{sic}\gamma = \frac{\gamma}{1 + \epsilon\Omega_r a_t \gamma}$, then when $\gamma \rightarrow \infty$ we get $\varpi = (\epsilon\Omega_r a_t)^{-1}$, substituting in (5) we obtain (7). This completes the proof. ■

From Corollary 2, it can be noticed that, in the case of imperfect SIC, the asymptotic BER does not depend on the SNR. Thus, the BER reaches a fixed value in the high SNR region, which indicates that the diversity gain is zero.

IV. NUMERICAL RESULTS

In this section, Monte Carlo simulations are presented to show the performance of the STAR-RIS-NOMA system, and to validate the BER analytical results derived in Section III. Unless stated otherwise, the distances from BS to STAR-RIS, STAR-RIS to U_t , and STAR-RIS to U_r are assumed, respectively as $d_{BS} = 50$ m, $d_{SU,t} = 6$ m and $d_{SU,r} = 4$ m. Additionally, the transmit power from the BS is normalized to unity, $P = 1$, and the power coefficients are allocated as $a_t = 0.7$ and $a_r = 0.3$. The path loss exponents associated with the BS-RIS and RIS- U_k links are given as $\alpha_{BS} = \alpha_{SU} = 2$. The RIS surface is uniformly partitioned into two parts, transmission and reflection parts, $N_t = N_r = \frac{N}{2}$. We compare the proposed system with the classical NOMA system by considering the same simulation parameters, furthermore, the BS- U_k path gain is modelled as $L_k = \frac{1}{d_k^\alpha}$, where d_k is the BS- U_k distance and $\alpha = 2$ is the path loss exponent.

Fig. 2(a)-(b) show the BER performance versus SNR in the case of perfect SIC and different numbers of transmitting/reflecting STAR-RIS elements, $N_k \in \{25, 50, 75\}$. It can be clearly seen that the obtained analytical results perfectly match the simulations curves, and the CLT approximation is shown to be accurate. It can be also seen that both users achieve better BER performance as the number of transmitting/reflecting elements increases. Compared to classical NOMA system, Fig. 2(b) shows that STAR-RIS NOMA (U_r) achieves 20 dB, 25 dB, and 29 dB performance gains for $N_r = 25, 50$ and 75, respectively at BER of 10^{-3} .

Fig. 3 shows the BER performance versus SNR for U_r with different SIC error propagation factors $\epsilon \in \{0, 0.03, 0.05\}$ and different numbers of reflecting STAR-RIS elements, $N_r \in \{25, 50, 75\}$. It is observed that the BER performance gets

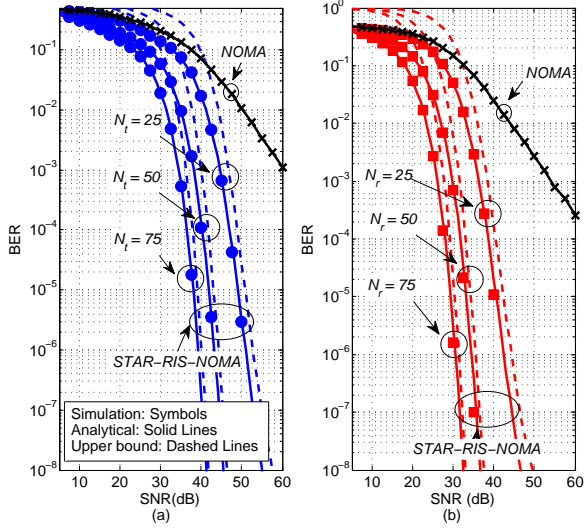


Fig. 2. The BER versus SNR for (a) U_t and (b) U_r in the perfect SIC case with different numbers of transmitting and reflecting RIS elements, respectively.

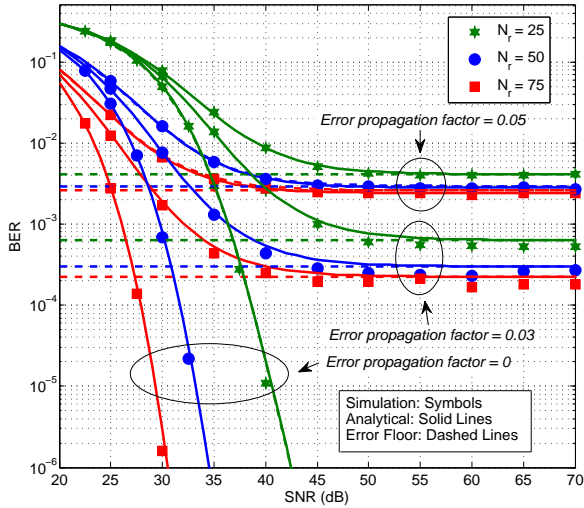


Fig. 3. The BER performance versus SNR for U_r in the imperfect SIC case, with different numbers of reflecting STAR-RIS elements.

worse as the SIC error increases and therefore, an error floor appears at the high SNR region.

Fig. 4 depicts the BER performance versus the number of transmitting/reflecting STAR-RIS elements for different power allocation coefficients. Here, $\gamma = 40$ dB. It can be seen from Fig. 4 that U_t is more sensitive to the change in the power allocation over the change of the number of transmitting/reflecting elements. This can be because U_t does not carry out any SIC process, and hence changes in the power allocation result in variations in the interference level caused by U_r . For instance, an increment of 0.1 in the power allocation makes U_t need 13 fewer elements to achieve the same BER of 10^{-3} . On the other side, U_r needs 3 elements more to achieve the same BER of 10^{-3} .

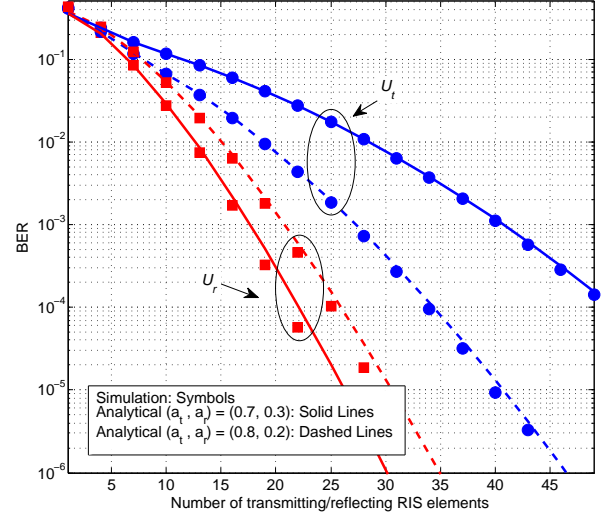


Fig. 4. The BER performance versus number of transmitting/reflecting STAR-RIS elements for different power allocation coefficients.

V. CONCLUSION

In this paper, we have examined the BER performance of the STAR-RIS-NOMA network, in which a STAR-RIS utilizes the mode switching protocol to provide communication between a BS and two NOMA users located on both its sides. Particularly, we have derived closed-form and upper bound expressions for BER in both perfect and imperfect SIC cases. Then, asymptotic analyses have been carried out to provide further insights into the error rate behavior in the high SNR region. Based on the numerical results, we conclude that the BER performance enhances with increasing numbers of STAR-RIS elements. Moreover, in the case of imperfect SIC, the BER performance gets worse and reaches a fixed value in the high SNR region, which indicates that the diversity gain is zero. On the other hand, in the case of perfect SIC, the users achieve diversity gain. Furthermore, the farthest user is more sensitive to changes in the power allocation over the change of numbers of transmitting/reflecting elements. Finally, it has been shown that the BER performance of STAR-RIS-NOMA outperforms that of the classical NOMA system and STAR-RIS based NOMA can be useful candidate for future systems. For a future work, the BER analysis provided here can be extended to the scenario where the STAR-RIS is partitioned between multiple users, and the aim is to find the minimum number of elements needs to be allocated for each user to guarantee a minimum BER threshold for all users.

APPENDIX A PROOF OF LEMMA 1

In what follows, we derive the BER in AWGN for U_t and U_r , separately and then unify them to achieve Lemma 1.

First, for U_t , given that U_t has the highest allocated power coefficient, then SIC is not required and U_r 's signal is treated as noise. The received signal at U_t is expressed as $y_t = \mathbf{g}_t^T \mathbf{\Theta}_t \mathbf{h}_t (\sqrt{a_t} P x_t + \sqrt{a_r} P x_r) + n_t$, where $\sqrt{a_r} P x_r$ denotes the interfering signal from U_r . Considering a binary phase shift keying (BPSK) modulation scheme, then we have

$y_t^+ = \mathbf{g}_t^T \Theta_t \mathbf{h}_t x^+ + n_t$ and $y_t^- = \mathbf{g}_t^T \Theta_t \mathbf{h}_t x^- + n_t$ when U_t 's symbol is $x_t = +1$ and -1 , respectively, where $x^+ \in \{\sqrt{a_t P} \pm \sqrt{a_r P}\}$ and $x^- \in \{-\sqrt{a_t P} \pm \sqrt{a_r P}\}$. Knowing that $n_t \sim \mathcal{CN}(0, \sigma^2)$, then $y_t^+ \sim \mathcal{CN}(\varphi_t x^+, \sigma^2)$ and $y_t^- \sim \mathcal{CN}(\varphi_t x^-, \sigma^2)$. Hence, the conditional error probabilities can be directly calculated by integrating the related PDFs of y_t^+ and y_t^- for each event in x^+ and x^- , and then can be written in terms of Q -function as $\mathcal{P}(e|\varphi_t, x^+) = \mathcal{P}(e|\varphi_t, x^-) = \frac{1}{2}Q((\sqrt{a_t} + \sqrt{a_r})\varphi_t\sqrt{\gamma}) + \frac{1}{2}Q((\sqrt{a_t} - \sqrt{a_r})\varphi_t\sqrt{\gamma})$ where $\frac{1}{2}$ is the probability of each event in x^+ and x^- . Finally, the BER for U_t in AWGN is calculated by $\mathcal{P}(e|\varphi_t) = \mathcal{P}(e|\varphi_t, x^+)\mathcal{P}(x^+) + \mathcal{P}(e|\varphi_t, x^-)\mathcal{P}(x^-)$. With equiprobable symbols, $\mathcal{P}(x^+) = \mathcal{P}(x^-) = \frac{1}{2}$, and we obtain $\mathcal{P}(e|\varphi_t) = \frac{1}{2}Q((\sqrt{a_t} + \sqrt{a_r})\varphi_t\sqrt{\gamma}) + \frac{1}{2}Q((\sqrt{a_t} - \sqrt{a_r})\varphi_t\sqrt{\gamma})$.

Second, for U_r , in order to detect its own signal, U_r needs to detect and subtract the signal of U_t . By considering imperfect SIC at U_r , then received signal of U_r is given by $y_r = \mathbf{g}_r^T \Theta_r \mathbf{h}_r \sqrt{a_r P} x_r + e_{sic} + n_r$. Here, the term of e_{sic} appears when SIC process is not being conducted perfectly and this results in a propagation error, which is modelled as a complex Gaussian RV, i.e., $e_{sic} \sim \mathcal{CN}(0, \epsilon \Omega_r P a_t)$. Considering BPSK modulation scheme, then we have $y_r^+ = \mathbf{g}_r^T \Theta_r \mathbf{h}_r x^+ + e_{sic} + n_r$ and $y_r^- = \mathbf{g}_r^T \Theta_r \mathbf{h}_r x^- + e_{sic} + n_r$ when U_r 's symbol is $x_r = +1$ and -1 , respectively, where $x^+ \in \{\sqrt{a_r P}\}$ and $x^- \in \{-\sqrt{a_r P}\}$. Likewise, the BER of U_r can be achieved by following same steps related to U_t except using $\sigma^2 = \sigma^2 + \epsilon \Omega_r P a_t$, and then $\mathcal{P}(e|\varphi_r) = Q(\sqrt{a_r} \varphi_r \sqrt{\frac{1}{1 + \epsilon \Omega_r a_t \gamma}})$. Now, by unifying $\mathcal{P}(e|\varphi_t)$ and $\mathcal{P}(e|\varphi_r)$, the BER for U_k in AWGN can be achieved in (3), and the proof is complete. ■

APPENDIX B PROOF OF LEMMA 2

φ_k can be written as $\varphi_k = |\sqrt{L_k} \sum_{n=1}^{N_k} \zeta_k^{(n)} \eta_k^{(n)} e^{j(\theta_k^{(n)} - \phi_k^{(n)} - \Phi_k^{(n)})}|$. For the two-user STAR-RIS network, the SNR can be maximized by letting $\theta_k^{(n)} = \phi_k^{(n)} + \Phi_k^{(n)}$, where the received signals from all the t and r STAR-RIS elements are constructively combined at U_t and U_r , respectively. Thus, after removing the channel phases, φ_k corresponds to the sum of the product of two independent Rayleigh RVs, where the mean and variance of the product are $\frac{\pi}{4}\sqrt{L_k}$ and $(1 - \frac{\pi^2}{16})L_k$, respectively. According to the central limit theorem (CLT), when $N_k \rightarrow \infty$, the cascaded channel φ_k follows Gaussian distribution, $\varphi_k \sim \mathcal{N}(\mu_k, v_k)$, where $\mu_k = \frac{\pi}{4}\sqrt{L_k}N_k$ and $v_k = (1 - \frac{\pi^2}{16})L_kN_k$. Hence, the PDF of φ_k can be finally expressed as in (4), which completes the proof. ■

APPENDIX C PROOF OF PROPOSITION 1

Unfortunately, the mathematical analysis of the BER become intractable when Lemmas 1 and 2 are substituted directly into the integration of (2). Hence, an alternative with a closed-form approximation is needed. A tighter and more tractable approximation of Q -function in Lemma 1 can be given by Lopez-Benitez and Casadevall, then $\mathcal{P}(e|\varphi_k) \approx$

$\sum_{\mathbb{A}_k} \mathcal{P}(\mathbb{A}_k) \exp(-a\mathbb{A}_k^2 \varphi_k^2 \varrho_k^{sic} \gamma - b\mathbb{A}_k \varphi_k \sqrt{\varrho_k^{sic} \gamma} - c)$ [18]. Next, substituting this approximation and Lemma 2 into (2), $\mathcal{P}_{e,k} \approx \frac{\exp(-\frac{2c\varphi_k + \mu_k^2}{2v_k})}{\sqrt{2\pi v_k}} \sum_{\mathbb{A}_k} \mathcal{P}(\mathbb{A}_k) \int_0^\infty \exp\left(-\frac{2a\mathbb{A}_k^2 \varrho_k^{sic} \gamma v_k + 1}{2v_k} x^2 - \frac{b\mathbb{A}_k \sqrt{\varrho_k^{sic} \gamma v_k} - \mu_k}{v_k} x\right) dx$. Here, the integral can be written in terms of error function [19, Eq. (3.322.2)]. Therefore, the BER of U_k can be finally stated in (5), and then the proof is complete. ■

REFERENCES

- [1] W. U. Khan *et al.*, "Spectral efficiency optimization for next generation NOMA-enabled IoT networks," *IEEE Trans. Veh. Technol.*, vol. 69, no. 12, pp. 15284-15297, Dec. 2020.
- [2] S. Islam *et al.*, "Power-domain non-orthogonal multiple access (NOMA) in 5G systems: potentials and challenges," *IEEE Commun. Surveys & Tuts.*, vol. 19, no. 2, pp. 721-742, 2nd quarter 2017.
- [3] Y. Liu *et al.*, "STAR: Simultaneous transmission and reflection for 360 coverage by intelligent surfaces," Mar. 2021. [Online]. Available: <https://arxiv.org/abs/2103.09104v2>.
- [4] C. Wu *et al.*, "Coverage characterization of STAR-RIS networks: NOMA and OMA," *IEEE Commun. Lett.*, June 2021.
- [5] T. Hou *et al.*, "A jointly design for STAR-RIS enhanced NOMA-CoMP networks: a simultaneously-signal-enhancement-and-cancellation-based (SSECB) design," May 2021. [Online]. Available: <https://arxiv.org/abs/2105.00404v2>.
- [6] J. Zuo *et al.*, "Joint design for simultaneously transmitting and reflecting (STAR) RIS assisted NOMA systems," June 2021. [Online]. Available: <https://arxiv.org/abs/2106.03001v1>.
- [7] W. Ni *et al.*, "STAR-RIS enabled heterogeneous networks: ubiquitous NOMA communication and pervasive federated learning," June 2021. [Online]. Available: <https://arxiv.org/abs/2106.08592v2>.
- [8] C. Zhang *et al.*, "STAR-IOS aided NOMA networks: channel model approximation and performance analysis," July 2021. [Online]. Available: <https://arxiv.org/abs/2107.01543v1>.
- [9] Z. Xie *et al.*, "STAR-RIS aided NOMA in multi-cell networks: a general analytical framework with Gamma distributed channel modeling," Aug. 2021. [Online]. Available: <https://arxiv.org/abs/2108.06704v1>.
- [10] Y. Liu *et al.*, "Simultaneously Transmitting and Reflecting (STAR)-RISs: A coupled Phase-Shift Model," Oct. 2021. [Online]. Available: <https://arxiv.org/abs/2110.02374v1>.
- [11] M. Aldababba, A. Khaleel and E. Basar, "Simultaneous transmitting and reflecting intelligent surfaces-empowered NOMA network," Oct. 2021. [Online]. Available: <https://arxiv.org/abs/2110.05311v1>.
- [12] J. Zuo *et al.*, "Uplink NOMA for STAR-RIS networks," Nov. 2021. [Online]. Available: <https://arxiv.org/abs/2110.05686v2>.
- [13] Z. Zhang *et al.*, "On the secrecy design of STAR-RIS assisted uplink NOMA networks," Nov. 2021. [Online]. Available: <https://arxiv.org/abs/2111.02642v1>.
- [14] C. Wu *et al.*, "Resource allocation in STAR-RIS-aided networks: OMA and NOMA," Nov. 2021. [Online]. Available: <https://arxiv.org/abs/2111.03883>.
- [15] Y. Guo *et al.*, "Energy-efficient design for a NOMA assisted STAR-RIS network with deep reinforcement learning," Nov. 2021. [Online]. Available: <https://arxiv.org/abs/2111.15464v1>.
- [16] J. Xu *et al.*, "STAR-RISs: A correlated T&R phase-shift model and practical phase-shift configuration strategies," Dec. 2021. [Online]. Available: <https://arxiv.org/abs/2112.00299v1>.
- [17] X. Yue *et al.*, "Simultaneously transmitting and reflecting reconfigurable intelligent surface assisted NOMA networks," Dec. 2021. [Online]. Available: <https://arxiv.org/abs/2112.01336v1>.
- [18] M. López-Benítez and F. Casadevall, "Versatile, accurate, and analytically tractable approximation for the Gaussian Q-Function," *IEEE Trans. Commun.*, vol. 59, no. 4, pp. 917-922, April 2011.
- [19] I. S. Gradshteyn and I. M. Ryzhik, *Table of integrals, series, and products*, 7th Ed. Academic Press: San Diego, CA, 2007.